Available online at www.sciencedirect.com
ScienceDirect
Combustion and Flame 150 (2007) 40–53
Combustion and Flame
www.elsevier.com/locate/combustflame

LES and experimental studies of cold and reacting flow in a swirled partially premixed burner with and without fuel modulation

A.X. Sengissen [a,*], J.F. Van Kampen [b], R.A. Huls [b], G.G.M. Stoffels [b], J.B.W. Kok [b], T.J. Poinsot [a,c,*]

[a] *CERFACS, 42 Avenue G. Coriolis, 31057 Toulouse cedex, France*
[b] *University of Twente, Faculty of Engineering, 7500 AE Enschede, The Netherlands*
[c] *IMFT, Avenue C. Soula, 31400 Toulouse, France*

Received 19 September 2006; received in revised form 29 January 2007; accepted 1 February 2007

Available online 18 May 2007

Abstract

In devices where air and fuel are injected separately, combustion processes are influenced by oscillations of the air flow rate but may also be sensitive to fluctuations of the fuel flow rate entering the chamber. This paper describes a joint experimental and numerical study of the mechanisms controlling the response of a swirled complex-geometry combustor burning natural gas and air. The flow is first characterized without combustion and LDV results are compared to large eddy simulation (LES) data. The nonpulsated reacting regime is then studied and characterized in terms of the heat release field. Finally the fuel flow rate is pulsated at several amplitudes and the response of the chamber is analyzed using phase-locked averaging and acoustic analysis. Results show that LES and acoustic analysis predict the flame dynamics in this complex configuration with accuracy when heat losses (radiation and convection) are accounted for.

Keywords: Flame transfer functions; Nonpremixed; Swirled; LES

1. Introduction

The ability to predict the stability of a given burner is the center of many present research programs. These efforts can be theoretical, experimental [1–12], or numerical [13–17]. A common specification of modern gas turbines is to operate in very lean regimes to satisfy emission regulations. The resulting flames can be sensitive to combustion oscillations, but the exact phenomena leading to instability are still a matter of discussion. A central question for modeling approaches is to know what induces an unsteady reaction rate (necessary to sustain the oscillations) when an acoustic wave enters the combustion chamber. This unsteady combustion process may be due to (at least) two effects (Fig. 1):

(1) The formation of vortices in the combustion chamber (Fig. 1a): These vortices are usually triggered by strong acoustic waves propagating

* Corresponding authors. Fax: +33 5 61 19 3030.
E-mail address: sengis@cerfacs.fr (A.X. Sengissen).

0010-2180/$ – see front matter
doi:10.1016/j.combustflame.2007.02.009

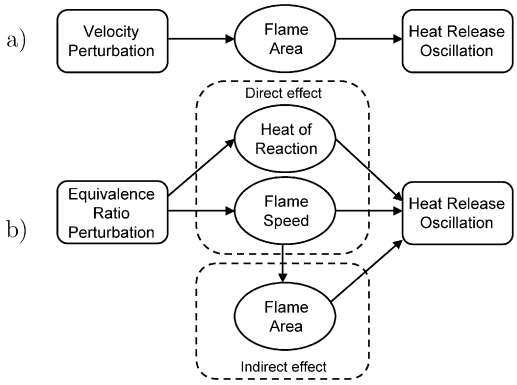

Fig. 1. Flame response to (a) velocity perturbations and (b) equivalence ratio perturbations.

in the air passages. These structures capture large pockets of fresh gases, which burn only later, in a violent process leading to small-scale turbulence and high reaction rates [18,19].

(2) The modification of fuel and oxidizer flow rates when the acoustic wave propagates into the fuel and air feeding lines (Fig. 1b). This can lead to local changes of the equivalence ratio and therefore to a modification of the burning rate when these pockets enter the chamber. If the burner operates in a very lean mode, this effect may be important, since variations of inlet equivalence ratio may trigger localized extinction and strong combustion oscillations [20].

In premixed combustors, the second mechanism has been identified as a key element controlling combustor stability [7,8,20] but its effects on nonpremixed devices remains unclear. According to Lieuwen [7,8], the mechanism is the following: even away from lean or rich blow off (LBO or RBO), equivalence ratio fluctuations produce heat-release oscillations that trigger combustion instabilities through acoustic feedback. A direct proof of the importance of fuel injection for stability is that the location of fuel injectors often alters the stability of the system. The crucial role of fuel modulation can also be readily identified by considering active control examples in which a small modulation of the fuel lines feeding a combustor can be sufficient to control the combustor [21–24].

Even though the general idea of the mechanism proposed by Lieuwen [7,8] is fairly clear, the details of the coupling phenomenon are still unknown. For instance, real instability mechanisms often mix mechanisms 1 and 2. A possible method for gaining more insights into this instability mechanism is to pulsate the fuel flow rate in a nonpremixed combustor. Multiple studies have examined the behavior of combustors submitted to a pulsation of the air stream to measure their transfer function [18,25,26]. Fewer data are available for fuel pulsation in imperfectly premixed devices [27]. Similarly, most numerical studies of flame responses have been performed on simple academic geometries. Clearly, being able to predict flame responses in real devices is a key issue for understanding combustion stability with complex geometries and a challenge for numerical methods.

The aim of this paper is to analyze the response of a swirled partially premixed combustor to a pulsation of the fuel flow rate. This combustor has a complex geometry, including swirlers, fuel injection by multiple jets, plenum, acoustic decoupler, and chimney, which are all meshed and computed. This constitutes one of the first attempts to numerically predict stability in a "stand alone" mode where boundary conditions cannot be tuned: the LES domain begins before the plenum, where the only condition is an imposed air-flow rate, and ends after the chimney, where pressure is imposed. This numerical effort is accompanied by two dedicated experimental studies on the same configuration (one with water for cold flow and another one for reacting flow). This 125-kW burner is installed at the University of Twente (The Netherlands) and is described in Section 2. The work is performed using large eddy simulation (Section 3) [9,14], a 3D Helmholtz solver to study acoustic modes (Section 4) [28,29], and several experimental methods (Section 5) [30,31].

The objective of this study is not to match the level of precision reached in state-of-the-art studies in the field of experimental methods for turbulent flames [32,33], LES development [34–37], or thermoacoustic modeling [38,39], but to use all these techniques simultaneously to study a realistic-geometry turbulent swirled burner submitted to acoustic perturbations. This is a mandatory step in addressing problems found in real combustors and to determine whether all critical phenomena appearing in complex burners are truly represented in simple academic situations. The following sections present validations of the LES and acoustic tools in terms of velocity fields for cold flow (Section 6), flame structure and position, noise spectra (Section 7), flame response to fuel forcing (evidenced qualitatively by flame positions under forcing but also quantitatively by the evolution of total heat release during one forcing cycle or by the response of the combustor to varying forcing amplitudes, Section 8). The overall message is that a "stand-alone" LES method combined with proper acoustic tools is able to predict the steady and forced behavior of a complex partially premixed combustor with reasonable accuracy. This holds for the present study and should hold for most reacting swirl flows, even though more validations are obviously needed.

2. Investigated configuration

2.1. Geometry

The test rig is a 125-kW lab-scale burner developed by the University of Twente (The Netherlands) and Siemens PG in the European Community project DESIRE (DESign and demonstration of highly REliable low NO_x combustion systems for gas turbines).

Fig. 2 presents the whole geometry, summarizes the flow path, and shows closer views of the various flow passages. Compressed, dried, and preheated air arrives in the air supply chamber and flows into the plenum through the acoustic decoupling system pipes (Fig. 2b). Downstream of the swirler (Fig. 2a), the air mixes with natural gas, which is injected at a normal angle into the air cross flow through four small holes, mimicking fuel injection in turbines. The mixture then reaches the combustion chamber, where the flame is stabilized, and burnt gases leave the chamber through the outlet flange (Fig. 2c). A channel ventilated with cooling air surrounds the combustion chamber in order to maintain wall temperatures in the range between $T = 900$ and 1200 K.

The LES computational domain (Fig. 2) includes all parts from the air supply chamber to the outlet flange. This is necessary to have the right acoustic impedance for the combustion chamber, to predict the chamber acoustic modes, and to minimize the uncertainties on boundary conditions. The cooling of the combustion chamber by convection and radiation is taken into account using a law-of-the-wall formulation for convection at solid walls and a gray gas model for radiation (Section 7.2).

2.2. Operating and boundary conditions

The reference operating point is the same for cold, reacting, and pulsated flows (Table 1). These conditions correspond to a lean regime and allow different levels of fuel flow rate forcing without choking injectors:

- The air supply feeds the chamber with 72.4 g/s of air, preheated to 573 K. This leads to a Reynolds number of 22,000 (based on the bulk velocity at the burner mouth and its diameter) and a swirl number [40] of 0.7 (at the same location).
- The natural gas is injected at ambient temperature (298 K) at a flow rate of 3.06 g/s. Note that the natural gas is replaced in the LES by methane (76.7% in mass) and nitrogen (23.3% in mass), so that the global equivalence ratio of the setup is 0.55.

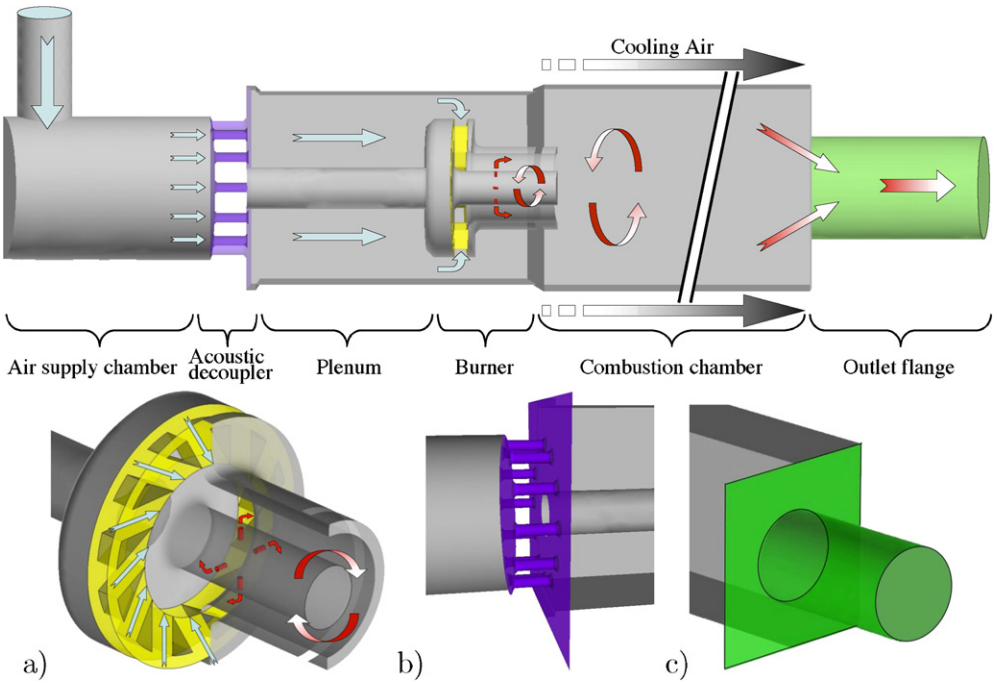

Fig. 2. Full LES computational domain, air flow (blue arrows), fuel injection (red arrows), and mixture path to the combustion chamber: (a) swirler vanes, (b) acoustic decoupling system, and (c) outlet flange. (For interpretation of the references to color in this figure legend, the reader is referred to the web version of this article.)

Table 1
Cases simulated and corresponding operating parameters

Case	AD_ COLD	AD_ STEADY	AD_ FORCE05	AD_ FORCE10	AD_ FORCE15	AD_ FORCE30	AD_ FORCE50	AD_ FORCE80	HL_ FORCE15	HL_ STEADY
Wall law	Adiabatic									Heat loss
$\dot{m}_A$	72.4 g/s at 573 K									
$\dot{m}_F$	N/A	3.06 g/s at 298 K								
F (Hz)	N/A	N/A	300 Hz							N/A
$\dot{m}'_F/\overline{\dot{m}_F}$	N/A	N/A	05%	10%	15%	30%	50%	80%	15%	N/A

- The mean absolute pressure of the test rig is 1.5 bar. It is imposed at the downstream end of the outlet flange (Fig. 2) using characteristic boundary conditions [41–43].

3. Large eddy simulations

The LES solver (www.cerfacs.fr/cfd/CFDWeb.html) simulates the fully compressible multispecies (variable heat capacities) Navier–Stokes equations on hybrid grids. Subgrid stresses are described using the Smagorinsky [44] model. When wall functions are used, this model gives results comparable to those for the dynamic model [45]. A two-step chemical scheme is fitted for lean regimes on the GRI-Mech V3 reference [46]. The fit procedure ensures that the two-step and GRI mechanisms produce the same flame speeds and maximum temperatures for laminar premixed one-dimensional flames [17] for equivalence ratios ranging between $\phi = 0.4$ and 1.2. The flame/turbulence interaction is modeled by the dynamic thickened flame (DTF) model [47] and allows to handle both mixing (which is important in partially premixed flames) and combustion. The numerical scheme uses second-order Lax–Wendroff [48] or third-order Taylor–Galerkin [49] spatial and third-order explicit (Runge–Kutta) time accuracy.

The boundary condition treatment is based on a multispecies extension [43] of the NSCBC method [41], for which the acoustic impedance can be controlled [42]. The walls are handled using a logarithmic law-of-the-wall formulation for velocity and temperature: the thermal treatment can be either adiabatic or "realistic," in which case a wall heat resistance is imposed (see Section 7.2). Typical runs are performed on grids between 900,000 and 2.7 million tetrahedra on several massively parallel architectures (SGI origin 3800, Compaq alpha server, Cray XD1) with a very efficient speedup.

4. Acoustic analysis

The Helmholtz solver is a useful tool for acoustic analysis in three-dimensional configurations [29,50–52]. It provides the eigenfrequencies of the configuration and the spatial structure of the corresponding eigenmodes. The Helmholtz solver needs a description of the geometry, the sound speed at every point, and the impedances at the boundaries. Here, the average sound speed field is provided by the average LES results (from temperature and species fields). The impedances imposed at the inlet and outlet correspond to a velocity and a pressure node, respectively.

5. Experimental diagnostics

5.1. Cold flow diagnostics

The laser Doppler velocimetry (LDV) equipment available at the University of Twente only allows low-velocity measurements. Consequently, the best way to validate LES with experimental data is to measure velocity profiles from a water tunnel experiment. The water tunnel is a geometrical copy of scale identical to that of the combustion test rig. The fluid is water instead of air. By choosing the water velocity to equate the Reynolds numbers in the water tunnel and the isothermal flow simulations, the two flows are similar.

The water tunnel is made out of Perspex, allowing forward scattering LDV to measure the velocity profiles downstream of the burner exit. The error of the system is less than 0.1% of its full measurement scale, whereas the resolution depends on the size of the measurement volume. A 400-mm focal length lens with a measurement volume of $6.5 \times 0.22 \times 0.22$ mm is used [53]. The measured velocity at a discrete point is the average velocity in the measurement volume. For all measured velocities, the axis of the measurement volume is aligned with the direction in which the velocity gradients are lowest, thereby increasing the resolution.

Data acquisition is done by a DIFA spectral analyzer installed on a PC. The transient velocity signals from the photomultipliers are sampled at 800 Hz for 40.96 s. Subsequently, the mean value and the variance of the 32,768 samples are determined. The power spectral density (PSD) of the measured signal shows that the sampling frequency is high enough to catch most of the phenomena in the flow; i.e., the PSD at 400 Hz is more than two orders of magnitude lower than the velocity amplitudes at lower frequencies.

To compare simulation results (using air as a medium) with water tunnel results the mean velocities and the variances are nondimensionalized by the bulk velocity at the burner mouth U_B and by $(U_B)^2$, respectively [53].

5.2. Hot flow diagnostics

The combustion process in the test rig can be observed optically through quartz glass windows mounted in the liner and pressure vessel on three sides of the combustion section. The view port size is 120 × 150 mm, which is large enough to see the whole flame zone.

The radical CH* is measured by chemiluminescence with a high-speed camera (Redlake) supplied with an intensifier (LaVision). A 430-nm bandpass filter (bandwidth of 10 nm) is used to filter the CH* radiation at the CH electronic band. The camera is gated for 100 μs and a movie of at least 100 images is recorded at 50 Hz. The images of the movie are corrected for background and nonlinear camera response and averaged.

A drawback of chemiluminescence is that no local flame behavior can be studied, since it is a line-of-sight technique, which means that the measured CH* concentration is the integral of all CH* in the line of sight of the camera. To compare with computations, LES fields have also been integrated along the line of sight.

Moreover, in terms of thermoacoustic measurements, the integrated CH* chemiluminescence measurements can be viewed as a direct measure of the volume-integrated heat release rate [30,54,55].

5.3. Acoustic diagnostics

To obtain the acoustic response of the system due to combustion, pressure measurements are made using Kulite pressure sensors. To decrease the thermal load on these sensors, they are placed in a sidetube ended by an anechoic tube. Furthermore, to allow high-pressure measurements, the backside of the sensor is connected to the pressurized rig using a long thin tube, which damps out all dynamic pressure signal on the back side, only providing a static back pressure. The pressure sensor signal is amplified and subsequently acquired using a Siglab data acquisition system at a sample frequency of 2.56 kHz.

6. Cold flow

LES and LDV data are first compared using one-dimensional velocity profiles on the central plane at several locations downstream of the burner exit (Plane_A: 5 mm, Plane_B: 15 mm, Plane_C: 25 mm, Plane_D: 45 mm, and Plane_E: 65 mm). The mesh contains 900,000 tetrahedral cells. The scale for all profiles in Fig. 3 is the same. Fig. 3 shows good agreement between experimental data and LES results in both shape and amplitude of the mean velocity components and their RMS fluctuations. The opening angle of the swirled jet, the intensity of the central recirculation zone, and the reattachment of the top/bottom recirculation zones are predicted correctly. No parameters (except the mesh) can be tuned to obtain these results: the flow through the swirler is resolved and no inlet profiles can be used for tuning in this setup.

7. Nonpulsated reacting flow

All reacting cases were computed on a 2.7-million-cell mesh especially refined in the region where the flame is expected to be and close to the fuel injectors to resolve the fuel jets properly.

7.1. Adiabatic cases

The steady-state reacting flow and the cold flow dynamics are very similar. The only noticable difference is the larger opening angle of the swirled jet. Fig. 4a exhibits the instantaneous three-dimensional flame structure, materialized by an isosurface of temperature at 1200 K. Even though the flame is compact, it is strongly wrinkled by the turbulence.

The mixing is characterized in Fig. 4b by the observed distribution function of local equivalence ratio ϕ (evaluated from the mixture fraction [56]), measured along the flame front. It confirms that mixing takes place before combustion, since very few points burn at equivalence ratio below 0.4 or above 0.7. The absence of stoichiometric reacting points also demonstrates that the flame never burns in a pure diffusion regime.

Fig. 5 displays the CH* field obtained experimentally and compares it to the heat release provided by LES, integrated along the line of sight. Both LES and experimental data show a very compact flame, with a length ($\simeq$80 mm) shorter than twice the diameter of the burner outlet.

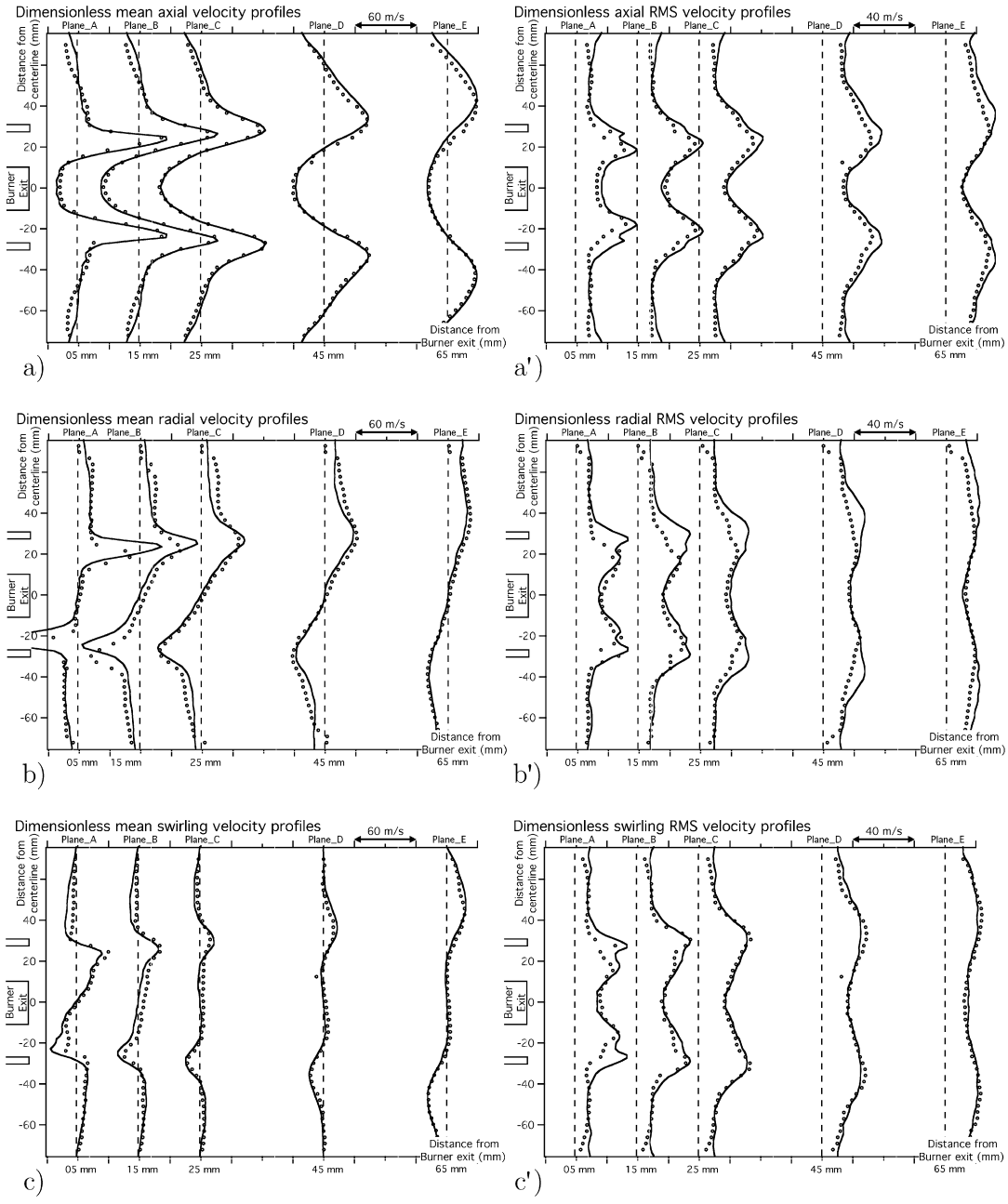

Fig. 3. Comparison of statistical profiles: (a) axial, (b) radial, and (c) swirling mean velocity; (a′) axial, (b′) radial, and (c′) swirling RMS velocity. (●) experiment; (—) LES; (- - -) zero line (case AD_COLD).

7.2. Nonadiabatic cases

Heat losses can play a significant role in combustion chambers, since both the reaction rate and the acoustics of the chamber are strongly linked to temperature. Adiabatic walls are a good assumption when the thermal barrier coating is efficient, e.g., when a ceramic heat shield is employed on the chamber walls [17]. In the present test rig, the thin metallic liner surrounded by the cooling channel invalidates that assumption, so that heat losses must be modeled.

In the experiment, the total heat loss to the cooling air can be calculated directly using the measured mass flow and temperatures at inlet and outlet. The total heat loss from the combustion chamber, Q_{Total}, is the sum of the heat loss to the cooling air, Q_1, and to

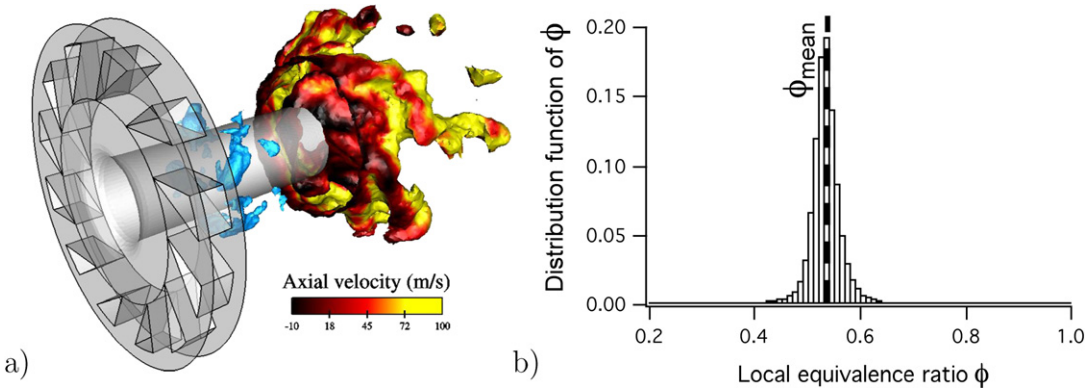

Fig. 4. (a) Instantaneous view of the flame (isosurface of temperature at 1200 K) and of the methane jets (isosurface of fuel mass fraction at 0.1); (b) equivalence ratio distribution function of the same instantaneous solution (PDF of case AD_STEADY) measured along flame front.

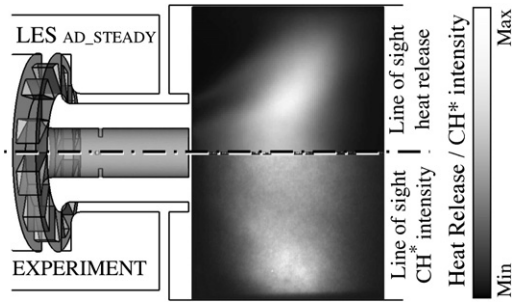

Fig. 5. Comparison of measured CH* intensity (bottom: experimental result) with heat release (top: LES result of case AD_STEADY) integrated over line of sight.

the surroundings, Q_2 (via the pressure vessel). Based on the adiabatic flame temperature and the measured temperature at the combustion chamber outlet, the total heat loss from the combustion gasses is rated at approximately 28% of the burner total power, e.g., 35 kW. The heat transferred to the surroundings, Q_2, is subsequently determined from the difference between the total heat loss and the heat taken by the cooling air:

$$Q_2 = Q_{\text{Total}} - Q_1. \tag{1}$$

In the LES, heat losses are computed by taking into account two phenomena (Fig. 6):

- Turbulent convection to the chamber walls. Heat transfer to the chamber walls is modeled using a law-of-the-wall function [57]. A simple conjugate approach is used for conduction though the walls and convection through air in the cooling channel. A global heat resistance R_w is used for these two mechanisms such that the local heat flux Q_w on any point on the walls is

$$Q_w = \frac{T_c - T_w}{R_w} \quad \text{with } R_w = \frac{d_c}{\lambda_c \text{Nu}} + \frac{d_w}{\lambda_w}, \tag{2}$$

where T_w, d_w, and λ_w are respectively the temperature, thickness, and conductivity of the wall, and T_c, d_c, and λ_c are the temperature, width, and conductivity of the cooling channel air. The Nusselt number Nu is given by a heat transfer correlation in the cooling channel,

$$\text{Nu} = 0.023\,\text{Re}^{4/5}\,\text{Pr}^{1/3}, \tag{3}$$

where Re is the Reynolds number of the cooling flow (Re = 5700). In all simulated cases, R_w is assumed to remain constant along the chamber wall and T_c to rise linearly along the combustion chamber axis from 300 to 575 K (values provided by experimental measurements).

- Radiation to the walls. Assuming that gases are optically thin, radiation can be modeled as a volumetric sink term calculated with a Stefan–Boltzmann law [58],

$$Q_r = \min\left(4\sigma\left(T^4 - T_s^4\right) p \sum_{k=1}^{n} (Y_k a_{p,k}),\ 0\right), \tag{4}$$

where T_s is the temperature of the surroundings (here T_s was set to 1500 K, a value close to wall temperatures), σ the Stefan–Boltzmann constant, and Y_k and $a_{p,k}$ are the mass fraction and Planck mean absorption coefficient for species k. These coefficients are obtained using the RADCAL program [59] and curve-fits provided by Gore et al. [60]. Such a simple procedure cannot be expected to compete with advanced radiation models [61,62], but its precision is sufficient for the present application.

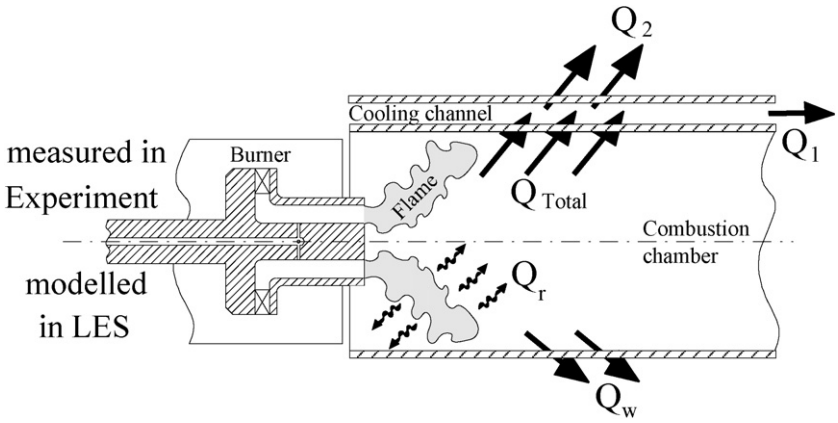

Fig. 6. Overview of the main heat loss phenomena measured in the experiment (top) and modeled in LES (bottom).

Table 2
Evaluation of the heat losses measured in the experiment and modeled in the LES

Fluxes	Experiment		LES	
	Cooling channel $Q_1 = 27$ kW	Casing $Q_2 = 8$ kW	Radiation $Q_r = 10$ kW	Convection $Q_w = 25$ kW
Q_{Total}	35 kW		35 kW	
T_{Outlet}	$\simeq$1300 K		$\simeq$1300 K	

Table 2 summarizes the measured heat fluxes in the experiment and the values resulting from the LES case HL_STEADY.

Now, comparing the field of heat release from LES with adiabatic (AD_STEADY) and nonadiabatic walls (HL_STEADY) shows that effects of heat losses on the mean flame shape are somehow limited. Its length and opening angle are very slightly increased, but the main effect of heat loss wall treatment is the modification of the acoustics of the chamber and will be introduced in the next sections.

7.3. Acoustic analysis

The acoustic eigenmodes of the setup can be computed using the 3D Helmholtz code [28,29,50,51] presented in Section 4. The field required for this analysis is the local mean speed of sound and is provided by a time-averaged solution of the reactive LES (cases AD_STEADY and HL_STEADY). Table 3 shows the lowest eigenfrequencies found numerically (see also Fig. 7) and compares them to the values measured in the experiment. All modes (Table 3) identified by the Helmholtz solver do not necessarily occur in the LES or the experiment. The two strongest modes found experimentally are at 433 and 820 Hz. Despite the coarse spectral resolution, these modes match very well the two modes found in the LES when heat losses are included (case HL_STEADY): 428 and 810 Hz. They are also very well recovered by the Helmholtz solver at 443 and 844 Hz. This confirms that these two modes are acoustically controlled and that they can be predicted accurately only when heat losses are accounted for.

Modes can be classified in three categories (Table 3). The "P" modes correspond to eigenfrequencies of the plenum and the "C" modes to eigenfrequencies of the chamber. Eigenfrequencies coupling the plenum and the chamber, thereby involving the full setup, are marked "S." For modes "P" and "C," this partial decoupling is possible because the inlet section of the chamber acts essentially like a velocity node. These results show that the two strongest modes (433 and 820 Hz) are acoustic modes of the chamber itself, but this is not a general result: many unstable combustors oscillate in modes involving the whole system or even only the plenum [63].

Fig. 8 also shows that beyond the expected effect of heat losses on the prediction of self-excited mode frequency, the impact on the eigenmode amplitude observed in LES is strong. Whereas the 480-Hz peak (Fig. 8, case AD_STEADY) is hardly distinguishable from the background noise (due to log scale), the corresponding 428-Hz peak (Fig. 8, case HL_STEADY) is much higher and closer to the measured level. In other words, by changing the mode frequency, the heat losses trigger a different flame response in the LES [64] and yield higher and more realistic pressure fluctuations levels.

Table 3
Eigenfrequencies computed by the Helmholtz code, measured in the experiment and in the LES

	Case	Eigenfrequencies (Hz)							
Helmholtz solver	Adiabatic	72	131	272	298	487	705	926	1093
	Heat loss	64	128	250	294	443	642	844	1045
Experiment	Measured	62	171		270	433	625	820	1022
LES	Adiabatic	X	X	X	X	480	X	920	X
	Heat loss	X	X	X	X	428	X	810	X
Mode	Description	1/4	3/4	5/4	7/4	5/4	7/4	9/4	1/2
	Related to	S	S	S	S	$C^{(a)}$	$C^{(b)}$	$C^{(c)}$	P

Note. 1/4, 3/4, ... designate quarterwave, three-quarterwave, ... modes related either to the "full setup" S, the "plenum" P, or the "chamber" C. Superscripts (a), (b), (c) indicate that this mode is represented in Figs. 7a, 7b, and 7c, respectively.

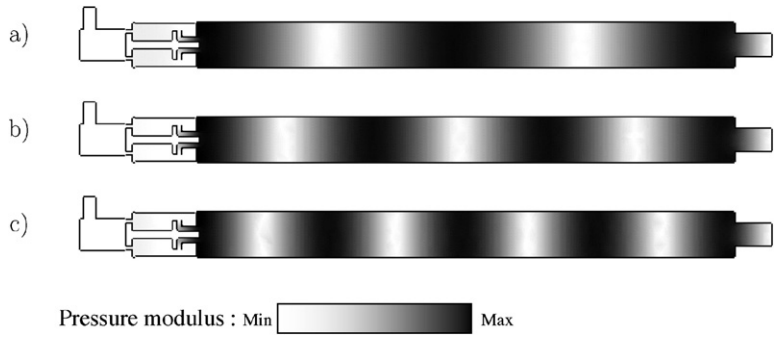

Fig. 7. Structure of the first eigenmodes of the combustion chamber given by Helmholtz solver: 487 (a), 705 (b), and 926 Hz (c). Acoustic pressure $|P'|$ in the central plane.

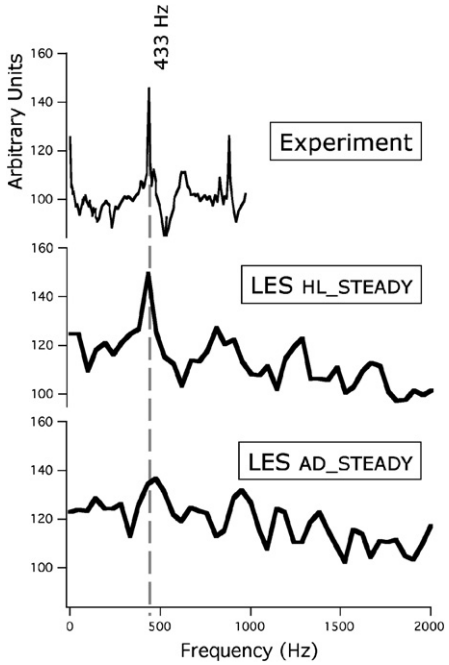

Fig. 8. Pressure spectra measured in the experiment (thin line) and computed with LES pressure signal (thick line) for cases AD_STEADY and HL_STEADY.

8. Pulsated reacting flow

8.1. Forcing method and phenomenology

Partially premixed combustors can be forced either through the air or the methane lines. Because of the acoustic decoupling system (Fig. 2b), the air flow rate is difficult to force in the present device and only the fuel line is pulsated in the experiment.

In the LES, forcing the reacting flow is achieved by pulsating the fuel mass flow rate (Fig. 2a) at 300 Hz for several amplitudes: 5, 10, 15, 30, 50, and 80% of the unforced mean mass flow rate. For all amplitudes, the fuel pipe flows remain subsonic, but the maximum Mach number can reach $M \approx 0.9$ in these pipes for case HL_FORCE80 (Table 1). The air flow rate remains constant and is only affected by the flow modulations induced by acoustic wave propagation. Section 8.4 will show that these modulations are not negligible.

In the experiment, fuel pulsation can have different forms. Some authors use a siren-like pulsator, i.e., with a rotating part [25,65,66]. An advantage of such actuators is their high maximum frequency of oscillation. The disadvantage is that the form of the excitation is fixed by the siren geometry.

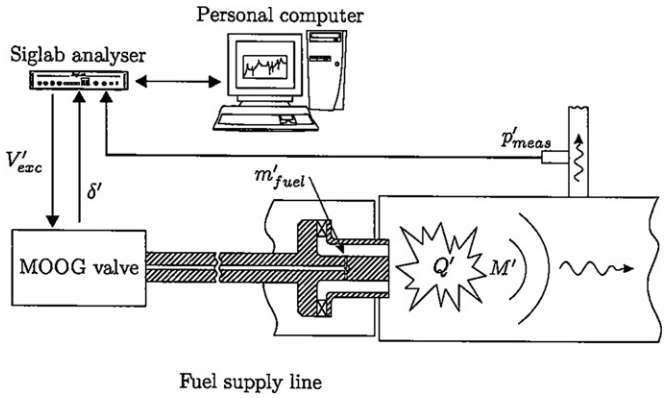

Fig. 9. Schematic layout of the method used in the unsteady measurements.

Another option is to use a control valve [21,27]. This type of actuator has a somewhat lower maximum frequency of oscillation, but it can generate any excitation signal. Since the maximum frequency of excitation is still high enough for the experiments performed here, a D633-7320 MOOG control valve is used in this study. The maximum level of excitation by the MOOG valve depends on the frequency and the operating point. At the reference operating point presented in Section 2.2 and at 300 Hz, the maximum forcing level is 12% of the mean fuel mass flow at the rim of the fuel pipes.

An overview of the different elements that play a role in the unsteady measurements is shown in Fig. 9. The MOOG valve is fed by a sinusoidal excitation signal, leading to a displacement of the MOOG's piston. To obtain the fuel mass flow perturbation at the fuel nozzles, the transfer function has been determined in a separate experiment. Hence, the fuel mass flow perturbation can be determined from the measured piston displacement. The fuel mass flow perturbation will cause a heat release perturbation, which can be detected by the optical measurements via the field of CH* radicals.

8.2. Acoustic analysis

Fig. 10 displays a typical pressure spectrum during forced operation at an excitation level of 15% at 300 Hz (cases AD_FORCE15 and HL_FORCE15). The self-excited mode at 433 Hz is still present and even increased by the forcing. As presented in Section 7.3, taking into account wall heat losses improves the prediction of both frequency and amplitude of the 433-Hz eigenmode. Moreover, the forcing frequency (300 Hz) is also noticeable in these spectra. The response of the flame to this forcing is studied in Sections 8.3–8.6.

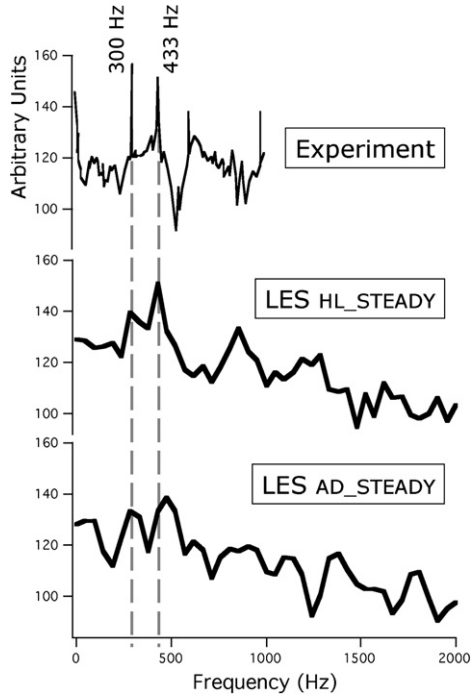

Fig. 10. Pressure spectra measured in the experiment (thin line) and computed with LES pressure signal (thick line) for cases AD_FORCE15 and HL_FORCE15.

8.3. Phase-locked averaged analysis

LES results can be phase-averaged (here on seven cycles) to isolate the flame response at 300 Hz. Fig. 11 displays the shape and intensity of the flame in eight phases of the cycle for the case HL_FORCE15. They also show the evolution of rich pockets along this cycle, materialized by an isosurface of equivalence ratio at $\phi = 0.6$ (slightly richer than the mean $\overline{\phi} = 0.55$). After a time lag of approximately 4 ms, these pockets reach the reacting zone. The flame does not move

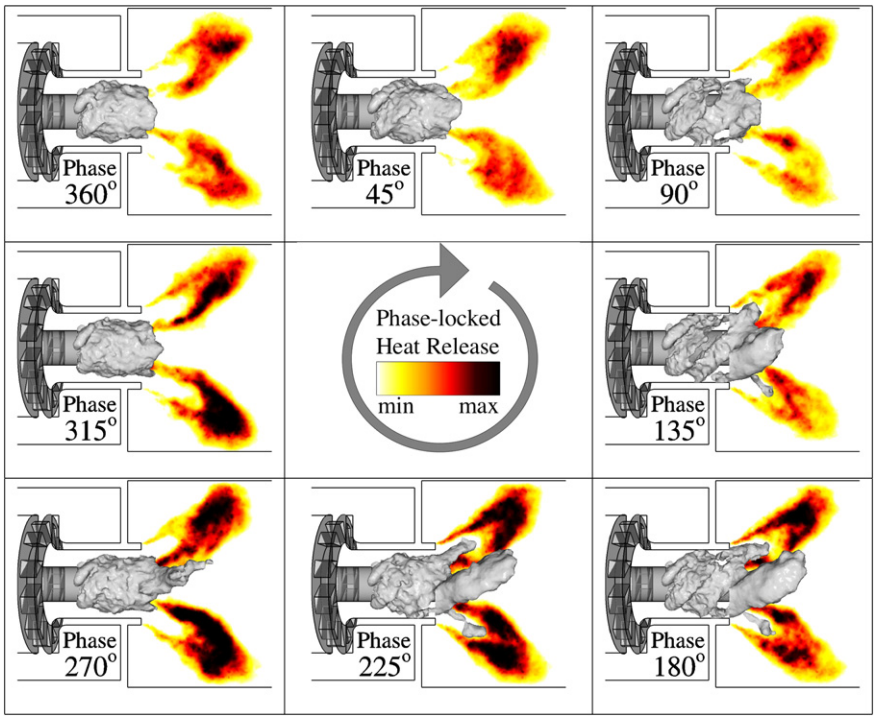

Fig. 11. Phase-locked heat release in the central plane and isosurface of equivalence ratio $\phi = 0.6$ for case HL_FORCE15.

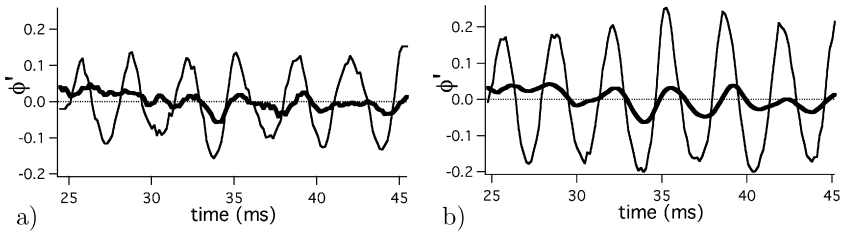

Fig. 12. Contribution of the fuel (thin line) and the air (thick line) fluctuations to equivalence ratio oscillations at the mouth of the burner for case AD_FORCE15 (a) and case AD_FORCE30 (b).

significantly when it is reached by these pockets, but the local heat release oscillates and triggers the pressure fluctuations feeding the 433 Hz acoustic mode (as described in Section 8.2).

8.4. Self-amplification of excitation

A controversial question in experiments where the fuel flow is pulsated is the following: is the air flow rate remaining constant during fuel flow rate pulsation? If it is, then only the direct mechanism in Fig. 1b has to be accounted for (equivalence ratio modulation due to fuel modulation). If the air flow rate does not remain constant, then both the direct and the indirect mechanism in Fig. 1b are important.

This can be checked in the LES by evaluating the fuel and air mass flow rates at the mouth of the burner. The variation of the equivalence ratio at the chamber inlet can be split in two parts (Eq. (5)), the contribution of instantaneous fuel flow rate to equivalence ratio fluctuations, ϕ'_{F}, and the contribution of instantaneous air flow rate to equivalence ratio fluctuations, ϕ'_{A}:

$$\phi' = \underbrace{\bar{\phi}\frac{\dot{m}'_{\mathrm{F}}}{\bar{\dot{m}}_{\mathrm{F}}}}_{\text{Fuel contribution } \phi'_{\mathrm{F}}} \underbrace{-\bar{\phi}\frac{\dot{m}'_{\mathrm{A}}}{\bar{\dot{m}}_{\mathrm{A}}}}_{\text{Air contribution } \phi'_{\mathrm{A}}} . \qquad (5)$$

Fig. 12 presents the two contributions ϕ'_{F} and ϕ'_{A} measured in the LES for two pulsation amplitudes: 15 and 30%. After a time delay of two cycles, the acoustic waves produced by the flame and partially reflected at the end of the chamber perturb the air flow rate. In other words, the $X\%$ pulsation of the fuel line

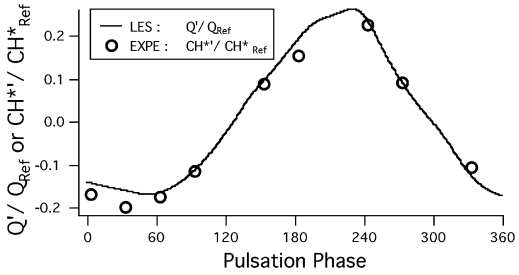

Fig. 13. Comparison of normalized global reaction rate fluctuations along the cycle (LES case AD_FORCE15: (—)) with normalized chemiluminescence fluctuations (experiment (●)).

is seen by the flame as a $1.2 \cdot X\%$ equivalence ratio excitation. In the present situation, the air flow is also affected by the fuel flow modulation and amplifies its impact on the fluctuations of equivalence ratio at the burner inlet. This conclusion is not general (it depends on the air line impedance) but shows that this effect should be taken into account for modeling.

8.5. Linearity of the flame response

Recent experimental results in studies of forced flames [67,68] show that beyond a certain pulsation amplitude, a saturation effect is observed. LES can be a good tool for evaluating the response of the flame up to high-amplitude excitations where measurements can be dangerous or even not feasible due to the limitations of the MOOG valve. For this reason as well, the LES case AD_FORCE15 will be compared to experimental results forced at 12%.

Fig. 13 first compares the level of reaction rate fluctuations (Q'/Q_{Ref}) observed in the LES (case AD_FORCE15) with the fluctuations of CH* radical ($\mathrm{CH}^{*\prime}/\mathrm{CH}^{*}_{\mathrm{Ref}}$) along the cycle. The mean values Q_{Ref} and $\mathrm{CH}^{*}_{\mathrm{Ref}}$ correspond to mean reaction rate (in the LES) and to mean CH* emission (in the experiment) for an unforced situation. Heat release Q and CH* emission are probably not linearly related for such a partially premixed flame so that comparing Q'/Q_{Ref} and $\mathrm{CH}^{*\prime}/\mathrm{CH}^{*}_{\mathrm{Ref}}$ is a challenging test. However, results show that both amplitude and phase are in quite good agreement, despite the limited number of cycles used in the LES phase-averaging procedure. Fig. 14 presents the reaction rate fluctuation level for several pulsation amplitudes (Fig. 14a), up to 80%, and its evolution along the cycle (Fig. 14b). The integrated CH* fluctuations are also displayed on Fig. 14a for low pulsation amplitudes. No saturation effect is noticed here: the flame behaves linearly from 0 to 80% forcing.

The difference between the present results and [67,68] may be due to the way the equivalence ratio is pulsated: in Balachandran et al. [67,68], the fuel flow rate is constant (fuel line choked) and they pulsate the air flow. Therefore, both mechanisms (1) and (2) are involved (see Section 1). Coherent structures (e.g., ring vortices) may wrinkle the flame and capture pockets of fresh gases [18]. In this study, since the momentum of the fuel jets is very small compared to the momentum of the air flow, only the second mechanism described in Section 1 (Fig. 1b) dominates.

8.6. Unsteady heat losses

In heavy-duty gas turbines, the thermal load on the walls is an important issue: on one hand, the air used to cool down either the metallic liner or the tile-holders of ceramic heat shield must be minimum to optimize the efficiency. On the other hand, even a temporary overheating may damage the structure and fluctuating heat load plays a crucial role in its long-term fatigue. Therefore, the mean thermal balance is not sufficient to predict this. Unsteady heat fluxes to walls must be investigated.

Fig. 15 presents the temporal evolution of global heat losses in the LES for both forced (HL_FORCE 15) and unforced (HL_STEADY) cases. The level of fluctuations of convective heat flux Q_{w} (Fig. 15a) as well as the radiative heat flux Q_{r} (Fig. 15b) are significantly increased by forcing. In all cases, approximately one-fourth of the total losses is due to radiation. Forcing the CH_4 lines leads to a fluctuation of the heat load on the wall (case HL_FORCE15).

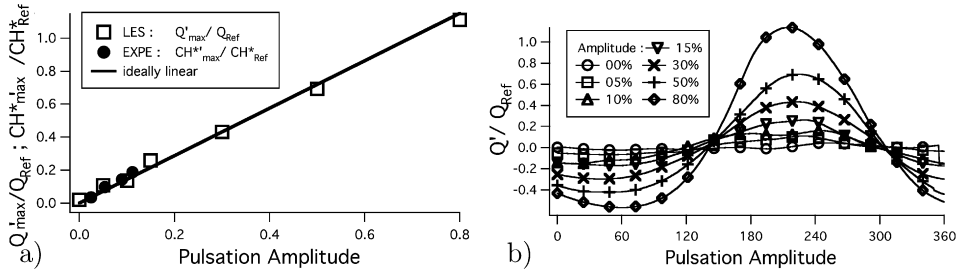

Fig. 14. Dependence of normalized global reaction rate fluctuations upon the forcing amplitude (a) and its evolution along the cycle (b).

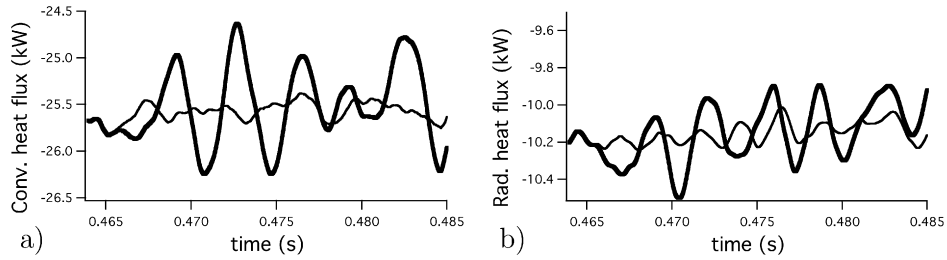

Fig. 15. Temporal evolution of (a) global convective Q_w and (b) radiative Q_r heat losses for cases HL_STEADY (thin line) and HL_FORCE15 (thick line).

Both convective and radiative fluxes oscillate by 10 and 4%, respectively. In addition to the noise level inside the combustion chamber, this can constitute a fundamental input data for a structure code.

9. Conclusion

This paper describes a joint effort where compressible large eddy simulation on unstructured grids and experimental tests on two rigs (one with water for cold cases and one with CH_4 and air for reacting conditions) were used to characterize the mean flow, the self-excited modes, and the forced response to fuel flow rate oscillation of a complex-geometry swirled combustor. The objectives were to understand the physics of self-excited and forced modes in such combustors but also to evaluate the capacities of LES to predict unsteady combustion in complex geometry burners:

- From a numerical point of view, results confirm recent studies [17,32,34,57] showing that LES can predict the mean flow (mean velocities and RMS values) in these swirled configurations accurately. In addition, in the framework of combustion instabilities, results show that LES can give access to the first self-excited modes with combustion. To achieve this, LES must be compressible and must be performed in a "standalone" mode to avoid ambiguity in boundary conditions in terms of mean flow and of impedances. An additional new result is the confirmation that heat losses must be accounted for in the LES because they control not only the sound speed (and therefore the frequency) but also the phase between heat release and pressure and therefore the amplitude of the modes. Radiation accounts for approximately one-fourth of heat losses in the present combustor. The analysis of LES and experimental results is also easier if a Helmholtz solver is used to predict all acoustic modes of the system.
- From a physical point of view, LES results suggest that the present combustor features partially premixed flames even though air and methane are injected separately: mixing upstream of the flame zone is strong enough to avoid any diffusion flames. The self-excited modes appearing with combustion are two acoustic modes of the combustion chamber itself. Under forced conditions, the flame reacts strongly and linearly to perturbations of the methane flow rate. No large-scale vortices are observed: the flame simply reacts to variations of equivalence ratio induced by fuel forcing. The flame response (total reaction rate versus phase angle) obtained by LES matches the experimental results obtained with CH^* chemiluminescence. Finally, LES reveals that pulsating the fuel flow in such a device also induces a fluctuation of the air flow rate which should be accounted for in instability models.

Acknowledgments

Most numerical simulations have been conducted on the computers of CINES, French national computing center, consuming about 40,000 h on an SGI origin 3800. This work was carried out in the framework of the EC project DESIRE coordinated by Siemens PG.

References

[1] S. Candel, Proc. Combust. Inst. 29 (2002) 1–28.
[2] F. Culick, AIAA J. 32 (1994) 146.
[3] A. Dowling, J. Sound Vib. 180 (1995) 557.
[4] A. Dowling, J. Fluid Mech. 394 (1999) 51.
[5] S. Ducruix, et al., J. Propuls. Power 19 (2003).
[6] W. Krebs, et al., Combust. Sci. Technol. 174 (2002) 99.
[7] T. Lieuwen, B. Zinn, Proc. Combust. Inst. 27 (1998) 1809.
[8] T. Lieuwen, J. Propuls. Power 19 (2003).
[9] T. Poinsot, D. Veynante, Theoretical and Numerical Combustion, second ed., R.T. Edwards, Philadelphia, PA, 2005.

[10] W. Polifke, A. Fischer, T. Sattelmayer, J. Eng. Gas Turb. Power 125 (2003) 20.
[11] T. Schuller, D. Durox, S. Candel, Combust. Flame 135 (2003) 525.
[12] T. Schuller, D. Durox, S. Candel, Combust. Flame 134 (2003) 21.
[13] H. Pitsch, L. Duchamp de la Geneste, Proc. Combust. Inst. 29 (2002) 2001.
[14] H. Pitsch, Ann. Rev. Fluid Mech. 38 (2006) 453.
[15] S. Roux, et al., Combust. Flame 154 (2005) 40.
[16] V. Sankaran, S. Menon, J. Turb. 3 (2002) 011.
[17] L. Selle, et al., Combust. Flame 137 (2004) 489.
[18] A. Giauque, et al., J. Turb. 6 (2005) 1.
[19] T. Poinsot, et al., J. Fluid Mech. 177 (1987) 265.
[20] J.H. Cho, T. Lieuwen, Combust. Flame 140 (2005) 116.
[21] C. Hantschk, J. Hermann, D. Vortmeyer, Proc. Combust. Inst. 26 (1996) 2835.
[22] K. McManus, T. Poinsot, S. Candel, Prog. Energy Combust. Sci. 19 (1993) 1.
[23] C. Paschereit, E. Gutmark, 37th AIAA Aerospace Sciences Meeting and Exhibit, edited by A.P. 99-0711, Reno, NV, 1999.
[24] T. Poinsot, et al., J. Phys. III July (1992) 1331.
[25] W. Cheung et al., ASME Paper, Atlanta, GA, USA, 2003.
[26] A. Kaufmann, F. Nicoud, T. Poinsot, Combust. Flame 131 (2002) 371.
[27] D. Bernier, et al., Combust. Sci. Technol. 175 (2003) 993.
[28] L. Benoit, Prédictions des instabilités thermoacoustiques dans les turbines à gaz, Ph.D. thesis, Université de Montpellier II, 2005.
[29] L. Benoit, F. Nicoud, Int. J. Numer. Methods Fluids 47 (2005) 849.
[30] H. Najm, et al., Combust. Flame 113 (1998) 312.
[31] N. Abel, J. Reine Angew. Math. 1 (1826).
[32] B. Janus, A. Dreizler, J. Janicka, Proc. Combust. Inst. 31 (2007) 3091.
[33] S. Kaiser, J. Frank, Proc. Combust. Inst. 31 (2007) 1515.
[34] O. Stein, A. Kempf, Proc. Combust. Inst. 31 (2007) 1755.
[35] H. El-Asrag, S. Menon, Proc. Combust. Inst. 31 (2007) 1747.
[36] M. Freitag, J. Janicka, Proc. Combust. Inst. 31 (2007) 1477.
[37] S. James, J. Zhu, M. Anand, Proc. Combust. Inst. 31 (2007) 1737.
[38] N. Noiray, et al., Proc. Combust. Inst. 31 (2007) 1283.
[39] S. Hemchandra, T. Lieuwen, Proc. Combust. Inst. 31 (2007) 1427.
[40] A. Gupta, D. Lilley, N. Syred, Swirl Flows, Abacus Press, 1984.
[41] T. Poinsot, S. Lele, J. Comput. Phys. 101 (1992) 104.
[42] L. Selle, F. Nicoud, T. Poinsot, AIAA J. 42 (2004) 958.
[43] V. Moureau, et al., J. Comput. Phys. 202 (2005) 710.
[44] J. Smagorinsky, Mon. Weather Rev. 91 (1963) 99.
[45] W. Cabot, P. Moin, Flow Turb. Combust. 63 (2000) 269.
[46] M. Frenklach, et al., Gas Research Institute Preprint, GRI-Report GRI-95/0058, 1995.
[47] J.P. Légier, T. Poinsot, D. Veynante, Summer Program 2000, Center for Turbulence Research, Stanford, USA, 2000, pp. 157–168.
[48] P. Lax, B. Wendroff, Comm. Pure Appl. Math. 13 (1960) 217.
[49] O. Colin, M. Rudgyard, J. Comput. Phys. 162 (2000) 338.
[50] C. Martin, et al., in: Proc. of the Summer Program, Center for Turbulence Research, NASA Ames/Stanford Univ., Stanford, 2004, pp. 377–394.
[51] C. Martin, et al., AIAA J. 44 (2006) 741.
[52] L. Selle, et al., Combust. Flame 145 (2006) 194.
[53] F. Rosendal, Swirling flows in expanding tubes, Ph.D. thesis, University of Twente, 1993.
[54] C.J. Lawn, Combust. Flame 132 (2000) 227.
[55] G.K. Mehta, M. Ramachandra, W. Strahle, Proc. Combust. Inst. 18 (1981) 1051.
[56] J.P. Légier, Simulations numériques des instabilités de combustion dans les foyers aéronautiques, Ph.D. thesis, INP Toulouse, 2001.
[57] P. Schmitt, et al., J. Fluid Mech. 570 (2007) 17.
[58] R. Barlow, et al., Combust. Flame 127 (2001) 2102.
[59] W. Grosshandler, NIST Preprint 1402 (1993).
[60] J. Gore, et al., in: Book of Abstracts of the 5th ASME/JSME Joint Thermal Engeneering Conference, American Society of Mechanical Engineers, New York, 1999, p. 50.
[61] T. Daguse, et al., Combust. Flame 106 (1996) 271.
[62] R. Goncalves dos Santos, et al., in: The Cyprus International Symposium on Complex Effects in Large Eddy Simulations, Springer, New York, 2005.
[63] K. Schildmacher, et al., Proc. Combust. Inst. 31 (2007) 3197.
[64] B. Schuermans, et al., ASME Turbo Expo GT2005-68393, 2005.
[65] A. Gentemann, et al., ASME Turbo Expo GT2004-53776, 2004.
[66] G. Richards, et al., J. Eng. Gas Turb. Power 119 (1997) 340.
[67] R. Balachandran, et al., Combust. Flame 143 (2005) 37.
[68] C.A. Armitage, et al., Combust. Flame 146 (2006) 419.